J Mater Sci: Mater Electron (2021) 32:25247–25257

A porous $ZnCo_2O_4$ nanosheets arrays as a binder-free electrode for high-performance flexible supercapacitor materials

Jing Wang[1,*], Chen Wang[1], Shen Wang[2], Xiang Zhang[3], Xiangyang Jin[1], Jiang Chang[1], and Jing Dong[1]

[1] School of Light Industry, Harbin University of Commerce, Harbin 150028, People's Republic of China
[2] MIIT Key Laboratory of Critical Materials Technology for New Energy Conversion and Storage, School of Chemistry and Chemical Engineering, Harbin Institute of Technology, Harbin 150001, People's Republic of China
[3] Institute of Composite Materials, Harbin Institute of Technology, Yikuang Street, Harbin 150001, People's Republic of China

Received: 23 February 2021
Accepted: 6 September 2021
Published online: 14 September 2021

ABSTRACT

In this paper, a porous $ZnCo_2O_4$ nanosheet arrays (NAs)/carbon cloth (CC) binder-free anode for the flexible energy storage devices application was constructed by the hydrothermal method and subsequent annealing treatment. This anode electrode material shows multistage pore distribution that can provide numerous ways for the transport of ions and electrons. As a supercapacitor electrode, the flexible $ZnCo_2O_4$/CC electrode indicates a high specific capacitance (1790 F/g at the current density of 1 A/g), good rate performance, and excellent cycle properties (99.4% capacitance retention after 10,000 cycles). Besides, the flexible electrode also displays good mechanical flexibility. A solid-state asymmetric flexible supercapacitor device was assembled with the $ZnCo_2O_4$/CC electrode as the positive electrode and the carbon nanotube (CNTs)/CC as the negative electrode. This asymmetric device delivers high energy density of 47.1 Wh/kg (power density 800 W/kg) and power density of 12,000 W/kg (energy density 28.3 Wh/kg) with the potential window 0–1.6 V. These results indicate that the $ZnCo_2O_4$/CC flexible electrode with high electrochemical performance adjusts for environment-friendly and low-cost energy storage devices in the future.

1 Introduction

With the rapid development of the flexible/bendable electronic device, flexible energy storage devices have attracted wide attention. Supercapacitors (SCs) are deemed to be one of the flexible energy storage devices due to their excellent electrical advantages such as long cycles, fast charge–discharge ability, high power density and so on [1–4]. But the insufficient energy density of SCs restricts their further

Address correspondence to E-mail: wangwangmayong@126.com

https://doi.org/10.1007/s10854-021-06982-4

application in daily life. The energy density is related to specific capacitance (C) and potential window (V) based on $E = 1/2CV^2$ [5–9]. For improving the energy density, the asymmetric supercapacitors device should be assembled by integrating different electrode materials. Meanwhile, the device will show a wide range of voltage window ($\sim$ 2 V) in aqueous electrolytes [10–15]. Hence, the preparation of high-performance electrode material with outstanding mechanical performance is an effective strategy to fabricate an excellent flexible SCs.

In recent years, binary metal oxides exhibit better pseudocapacitor electrochemical properties than the single component metal oxides because of their higher electronic conductivity, higher theoretical capacity, and reversible redox reactions [16–21]. For example, Swapnil et al. reported that $RuCo_2O_4$//rGO hybrid supercapacitor cell demonstrates the specific capacity of 372 mAh/g [22]. Shipra Raj et al. reported that $NiCo_2O_4$ shows the specific capacitance of 80 F/g^- at current density of 0.1 A/h [23]. Pragati et al. reported that the $CoMn_2O_4$@NiCo–OH delivers a high specific capacity of 349 mA/g [24]. Among the various binary metal oxides, $ZnCo_2O_4$ materials as active materials for supercapacitors are reported to be promising electrode materials due to their better electrochemical performance, higher conductivity, low cost, and environmental friendliness [25, 26]. Such as Swati et al. prepared $ZnCo_2O_4$ microstrips/carbon cloth, which displayed a good cycling performance and 94% capacity retention over 10,000 cycles in 1 M KOH aqueous electrolyte [27]. Liu et al. synthesized the three-dimensional $ZnCo_2O_4$ nanowire arrays/carbon cloth anode for Li-ion battery and showed high reversible capacitance of 1300–1400 mAh/g [28]. Wu et al. prepared $ZnCo_2O_4$ nanorod arrays/carbon cloth and the $ZnCo_2O_4$-CC//PPy-CC asymmetric supercapacitor device displayed an energy density of 2.3 mW h/cm^2 at the power density of 18.9 mW h/cm^3 [29]. Therefore, a simple and mild route to construct high-performance $ZnCo_2O_4$ flexible electrode is important for realizing the practical application of flexible energy storage electronic devices.

In this paper, we prepared the porous $ZnCo_2O_4$ nanosheet arrays grown directly on the surface of the flexible carbon cloth using one-step simple hydrothermal method with heat treatment. These nanosheets showed that the porous structure connected with each other form numerous holes, which are contributed to the electrolyte ion and electrons transportation among the interface and surface of the materials. Given this the binder-free electrode showed high specific capacitance of 1790 F/g at the current density of 1 A/g, rate property of 68%, and cycling performance with the capacitance retention of 99.4%. The asymmetric supercapacitors device was assembled taking the porous $ZnCo_2O_4$ nanosheets arrays as the positive and the carbon nanotubes as the negative. The device displays a wide potential window of 1.6 V, high energy density of 47.1 of Wh/kg (at the power density of 800 W/kg), and excellent cycling performance.

2 Experiments

In the experiments, the reagents were used with analytical grade and did not need further purification. Carbon cloth ($1 \times 1 \times 0.1$ cm^3) was used as conductive collector and cleaned by sonication method in the 6 M HNO_3, ethanol, and deionized water for about 1 h, respectively.

2.1 The preparation of the porous $ZnCo_2O_4$ NAs/CC electrode

The porous $ZnCo_2O_4$ NAs were prepared directly grown on carbon cloth by one pot hydrothermal method. Firstly, 0.8 mmol $Zn(NO_3)_2{\cdot}6H_2O$, 2.5 mmol $Co(NO_3)_2{\cdot}6H_2O$, 3 mmol $CO(NH_2)_2$, and 1.5 mmol NH_4F were mixed in 30 mL of deionized water with sonication for 3.5 h. The above mixtures were transferred into a 50 mL Teflon-lined stainless-steel autoclave with a piece of cleaned carbon cloth. The autoclave was sealed and maintained at 150 °C for 6 h. Then the samples were cooled down to the room temperature, taken out, and cleaned with ethanol and the deionized water for three times and dried at 50 °C for 8 h, followed by annealing at 550 °C in air for 5 h. Finally, the porous $ZnCo_2O_4$ NAs/CC electrode was obtained ($\sim$ 1 cm^2 area; $ZnCo_2O_4$ NAs mass: 2.1 mg).

2.2 The preparation of carbon nanotubes (CNTs)/CC electrode

The CNTs/CC electrode was prepared as follows: firstly, 0.5 g CNTs were taken and dropped in 60 mL 80% HNO_3. Then the mixture was heated at 80 °C for 18 h followed by constant stirring. When the

mixtures are cooled down to room temperature, the CNTs were cleaned with ethanol and deionized water for three times, respectively, and dried at 50 °C for 10 h. The CNTs/CC electrode was prepared by mixing CNTs (80 wt%), carbon black (10 wt%), and polyvinylidenefluoride (PVDF, 10 wt%). A small amount of ethanol was then added to the above mixtures. These mixtures were coated onto the surface of CC and dried at 90 °C for 6 h.

2.3 The preparation of the gel-state asymmetric supercapacitors

The asymmetric supercapacitors device was assembled by using $ZnCo_2O_4$/CC electrode as positive and CNTs/CC electrode as negative. PVA/KOH was used as the gel-state electrolyte. PVA/KOH gel electrolyte was synthesized by mixing KOH 2.8 g and PVA 3 g into 25 mL deionized water and then heated at 80 °C and stirred for 5 h. The two electrodes and the separator were soaked in PVA/KOH gel electrolyte for a few minutes. Then they were taken out from the gel and assembled together. The device was placed in air for 12 h and became solid state. The electrochemical properties of the device were tested by an electrochemical CHI 660E workstation, made in Shanghai, China. The electrochemical tests of the as-prepared electrodes were firstly performed in a three-electrode system with 2 M KOH as electrolyte. Pt plate was used as the counter electrode and the saturated calomel electrode (SCE) was used as the reference electrode. Cyclic voltammetry (CV), Galvanostatic charge–discharge (GCD), and electrochemical impedance spectroscopy (EIS, 0.01–100 kHz with an amplitude of 5 mV) were firstly tested in a three-electrode cell, the capacitance was calculated as follows:

$$C_m = I\Delta t/m\Delta V \quad (1)$$

C_m (F/g) is the specific capacitance of a single electrode. I (A) represents the current of discharge, and Δt (s) is the discharge time. m (g) is the mass of the active material and ΔV (V) is the potential window.

The electrochemical measurements of the device of the energy density (E) and power density (P) are calculated from the following equation:

$$E = 1/2CV^2 \quad (2)$$

$$P = W/\Delta t(s) \quad (3)$$

2.4 Materials characterization

The morphology of the as-prepared samples was examined by scanning electron microscopy (SEM, JEOL JSM-7500F) and transmission electron microscopy (TEM, JEOL JEM-2100F). The crystal structures of the as-prepared materials were observed by X-ray diffraction (XRD, RigakuD/max-2600 PC) with the Cu Ka radiation (1.5406 Å). The electrochemical tests were performed by a Shanghai Chenhua CHI660E electrochemical workstation.

3 Results and discussion

The morphology of the as-prepared samples was tested by SEM. Figure 1a shows the carbon cloth with the diameter of 15 μm for a single carbon fiber. After a simple one-step hydrothermal process with heat treatment, the as-prepared $ZnCo_2O_4$ NAs with high density are uniformly grown on the surface of the carbon fibers as shown in Fig. 1b. The magnified image of Fig. 1c indicates a large number of $ZnCo_2O_4$ NAs grown on the carbon fiber. Figure 1d further confirms that $ZnCo_2O_4$ NAs have the thickness of 10 nm and these nanosheets are connected with each other forming porous structures. Further taking the hole section of Fig. 1d for SEM mapping, the results indicate the existence of Zn, Co, O, and C elements as shown in Fig. 1e. Figure 1f shows the corresponding EDS tests, indicating that the Zn, Co, O, and C elements can be found. These results are consistent with Fig. 1e SEM mapping tests.

The microstructures of the as-prepared products were further detected by TEM tests. From Fig. 2a, these nanosheets are some porous structures and these nanosheet arrays connected with each other forming holes can be found. The mesoporous properties of the thin nanosheets are generally attributed to the re-crystallization reaction and the liberation of gas during the thermal treatments. Figure 2b demonstrates the lattice spacing of 0.23 nm and 0.24 nm, corresponding to the (222) and (311) lattice planes of $ZnCo_2O_4$. The inset in Fig. 2b shows the corresponding selected area electron diffraction (SAED) patterns, indicating the polycrystalline properties of the as-prepared samples. Further taking the section of Fig. 2a for TEM mapping as shown in Fig. 2c, Zn, Co, O, and C elements still can be found. These results are consistent with the SEM mapping

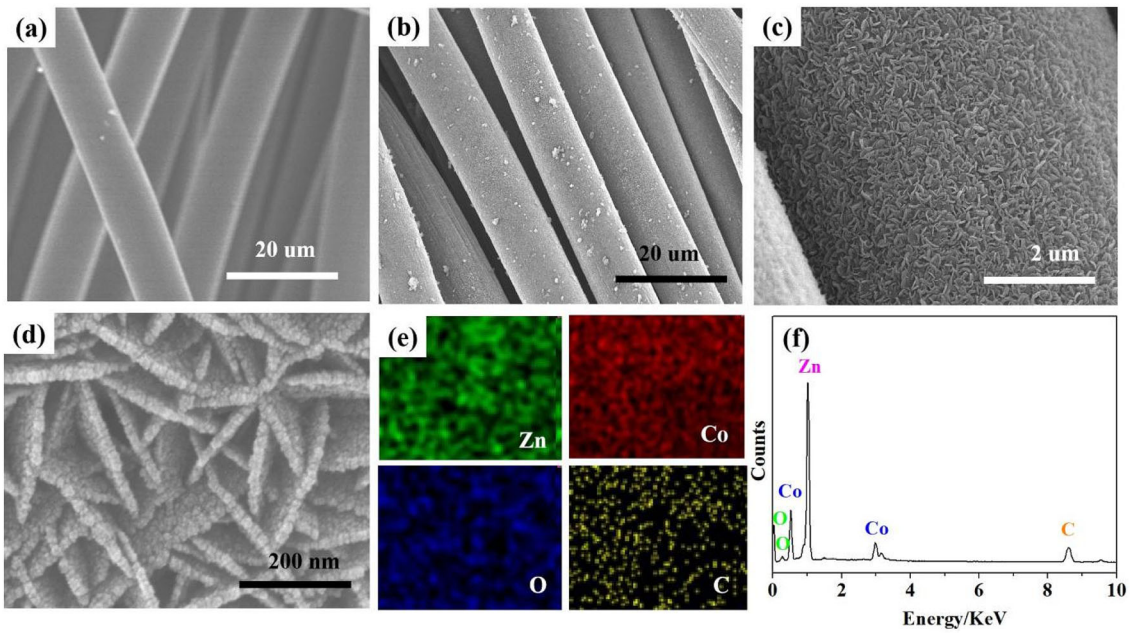

Fig. 1 SEM images of carbon cloth (**a**) and $ZnCo_2O_4$ NSs/CC (**b**–**d**) at different magnifications; SEM mapping images (**e**) and EDS spectrum (**f**) of $ZnCo_2O_4$ NSs/CC

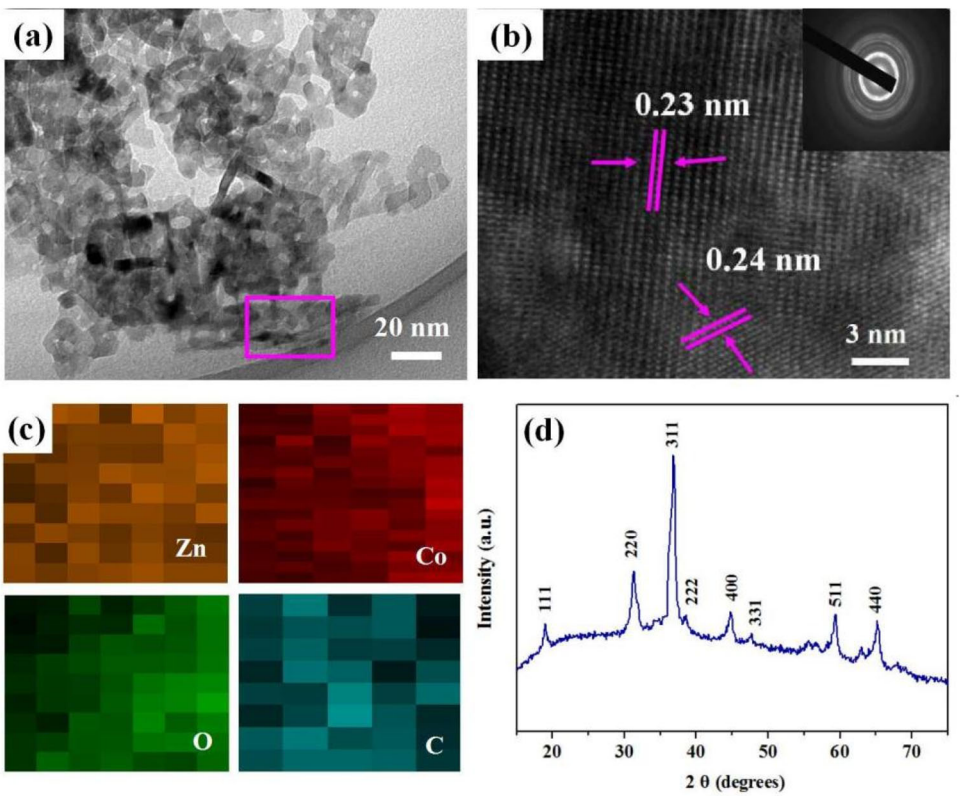

Fig. 2 **a** TEM image, **b** HRTEM image of the pink box from (**a**), and the inset is the corresponding SAED pattern. **c** TEM mapping images of the pink box from (**a**), and **d** XRD patterns of $ZnCo_2O_4$ NSs (Color figure online)

tests and EDS tests. The crystal structures of $ZnCo_2O_4$ were detected by X-ray diffraction (XRD) tests in Fig. 2d, which confirms the $ZnCo_2O_4$ (JCPDS Card No. 23-1390). The porous structure of $ZnCo_2O_4$ nanosheets was further researched by BET (Brunauer–Emmett–Teller) N_2 adsorption desorption

tests. The results are shown in Fig. 3. $ZnCo_2O_4$ nanosheets display the specific surface area of 116.86 m^2/g. This porous configuration is mainly due to the porous structure of $ZnCo_2O_4$ and the interconnected $ZnCo_2O_4$ nanosheets grown directly on the carbon cloth nanofibers scaffold. The special nanosheets structures display not only large specific surface area and high electrolyte permeability, but also allow fast ion and electron transportation.

The electrochemical performances of the $ZnCo_2O_4$ NAs/CC are firstly tested in a three-electrode system with 2 M KOH as the electrolyte to study the potential application of the flexible electrode. The CV curves of carbon cloth (CC) and $ZnCo_2O_4$ NAs/CC at the scan rate of 5 mV/s are shown in Fig. 4a. The results demonstrated that the porous $ZnCo_2O_4$ NAs/CC electrode shows higher capacity performances than the pure carbon cloth, which indicates that the pure carbon cloth contributes hardly to the capacitance of the porous $ZnCo_2O_4$ NAs/CC electrode. Figure 4b exhibit the charge–discharge curves of carbon cloth and $ZnCo_2O_4$ NAs/CC electrode at the current density of 3 A/g. The discharge time of $ZnCo_2O_4$ NAs/CC electrode is longer than carbon cloth. According to Eq. 1, the specific capacitances of carbon cloth and $ZnCo_2O_4$ NAs/CC electrode are calculated at the same current density of 3A/g and are shown in Fig. 4c. The results further confirm that the carbon cloth (30 F/g) shows little performance to the total capacitance of $ZnCo_2O_4$ NAs/CC electrode (1560 F/g). Figure 4d exhibits the CV curves of $ZnCo_2O_4$ NAs/CC electrode at different scan rates

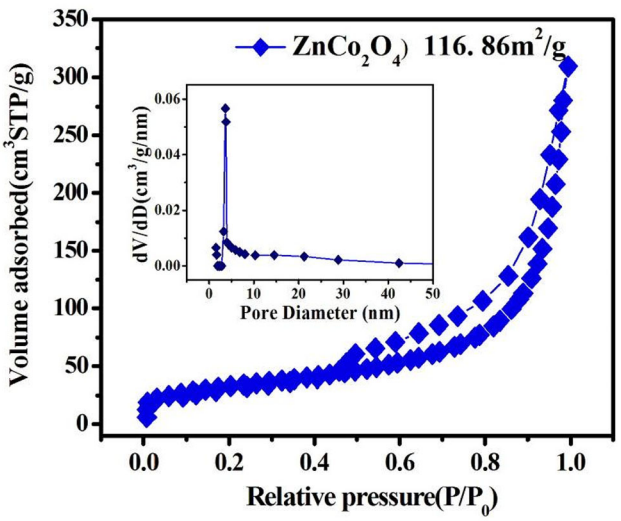

Fig. 3 N_2 adsorption–desorption tests of $ZnCo_2O_4$ nanosheets

from 10 to 100 mV/s. The CV curves indicate the pseudocapacitance properties of $ZnCo_2O_4$ NAs and the curves remain basically the same as the scan rate increases, demonstrating the good reversibility. When the scan rate increases, the peak current increases indicating the fast electron and ionic transportation of the as-prepared $ZnCo_2O_4$ NAs/CC electrode. Charge–discharge curves were also tested at different current densities of 1, 2, 5, 10, 15, and 20 A/g in Fig. 4e. These charge–discharge curves with good symmetry revealed the desirable electrochemical reversibility. The specific capacitance properties of the $ZnCo_2O_4$ NAs/CC electrode were calculated: 1790, 1620, 1450, 1360, 1290, and 1120 F/g at the current density of 1, 2, 5, 10, 15, and 20 A/g, respectively, as shown in Fig. 4f. The porous $ZnCo_2O_4$ NSs/CC electrode with a high specific capacitance at the current density of 1 A/g is higher than the hexagonal $ZnCo_2O_4$ electrode (846 F/g) [26], core–shell $ZnCo_2O_4$@$NiCo_2O_4$ structures (1476 F/g) [30], and the porous $ZnCo_2O_4$ hollow spheres (1150 F/g) [31]. And the specific capacitance of 1120 F/g at a high current density of 20 A/g is also higher than the core–shell $ZnCo_2O_4$@$NiCo_2O_4$ electrode (942 F/g) [30], mesoporous $ZnCo_2O_4$ microspheres (830 F/g) [32], the carbon nanofiber@$ZnCo_2O_4$ (940 F/g) [33], and the $ZnCo_2O_4$/ZnO@multiwall carbon nanotube (1705 F/g) [34]. These results show the good electrochemical activities of the as-prepared porous $ZnCo_2O_4$ NSs/CC electrode. A cycling test was examined at the current density 2 A/g for 10,000 cycles as shown in Fig. 4g. The specific capacitance of $ZnCo_2O_4$ NAs/CC electrode changes from 1620 to 1610 F/g, which keeps the capacitance retention of 99.4%. SEM and TEM images of the as-prepared electrode after 10,000 cycles are provided as shown in Figs. 5 and 6, respectively. These results indicate that the as-prepared $ZnCo_2O_4$ materials have good structural stability, and the morphology also keeps consistent after 10,000 cycles. We compare our work with the as reported specific capacitance and cycling performance of the reported other binary oxides. $ZnCo_2O_4$-based electrodes and the present work are shown in Table 1.

Figure 4h shows the last 10th cycle tests of charge–discharge curves. The charge–discharge curves are consistent without obvious changes, indicating good cycle properties. The Nyquist plots of the $ZnCo_2O_4$ NAs/CC electrode after 1st and 10,000th cycles are detected in Fig. 4i. The arc increments are no obvious

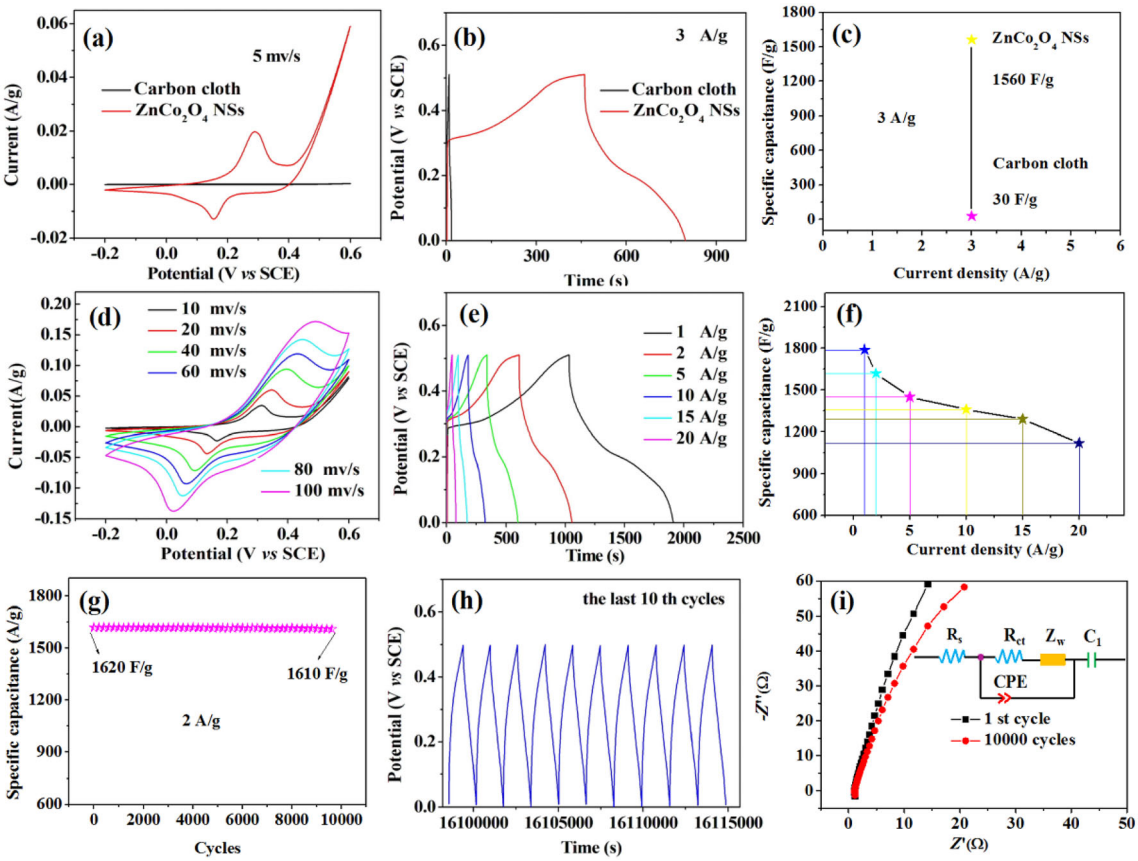

Fig. 4 **a** CV curves, **b** charge–discharge curves, and **c** specific capacitance of the carbon cloth and $ZnCo_2O_4$ NSs/CC; **d** CV curves, **e** charge–discharge curves, and **f** specific capacitance of $ZnCo_2O_4$ NSs/CC; **g** cycling performance of $ZnCo_2O_4$ NSs/CC at the current density of 2 A/g; **h** the last 10th cycles of $ZnCo_2O_4$ NSs/CC; and **i** Nyquist plot of $ZnCo_2O_4$ NSs/CC

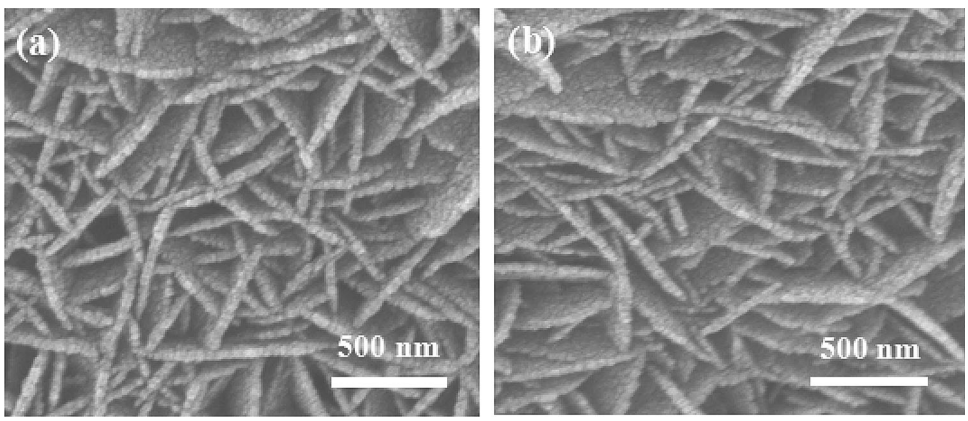

Fig. 5 SEM images of the electrode: **a** the first cycle and **b** after 10,000 cycles

difference indicating the structures well maintained with 10,000 cycles. Further, enlarged Nyquist plots are shown in Fig. 7. The slope of the curve is the Warburg impedance increased after 10,000 cycles, attributing to the loss of a few active materials during the charge and discharge process. Rate and cycle performance of the hybrid $ZnCo_2O_4$ NAs/CC electrode under different current densities as shown in Fig. 8. After changing the current density at different forms and returning to the original forms, the specific capacitance is basically unchanged.

Figure 9a shows the image of the as-prepared $ZnCo_2O_4$ NAs/CC electrode with the size 1 × 1 cm^2. The CV curves in four twisting and bending forms

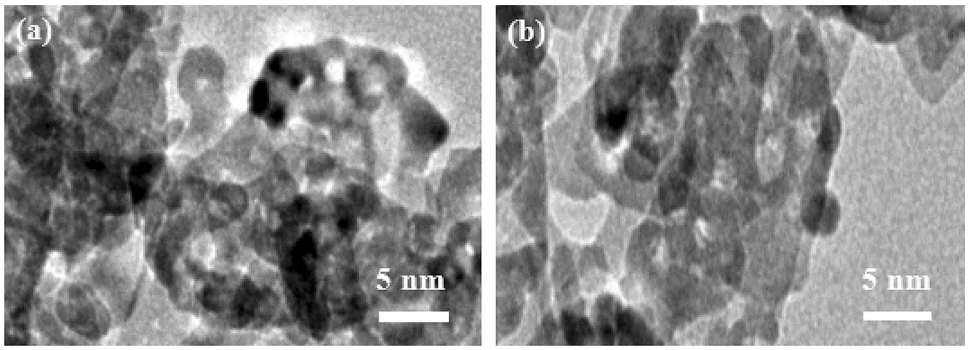

Fig. 6 TEM images of the electrode: **a** the first cycle **and b** after 10,000 cycles

Table 1 Comparison of specific capacitances and cycling performance of the reported other binary oxides, $ZnCo_2O_4$-based electrodes, and the present work

Electrode materials	Current density	Capacitance (F/g)	Cycles	Retention (%)	Refs.
$ZnCo_2O_4$ nanorod	2 mA/cm^2	305	3500	92	[35]
$NiMoO_4$ nanosheet	5 A/g	847.7	10,000	89.2	[36]
$CoMoO_4$–$NiMoO_4{\cdot}xH_2O$ bundles	2.5 mA/cm^2	1039	1000	72.3	[37]
$NiMoO_4$ nanoflake	5 mA/cm^2	131.8	6000	94.2	[38]
$ZnCo_2O_4$ microspheres	1 A/g	647.1	2000	91.5	[39]
$NiMoO_4$/$CoMoO_4$ nanorods	1 A/g	1445	3000	78.8	[40]
$NiCo_2O_4$@$NiMoO_4$	2 mA/cm^2	1389	2000	90.6	[41]
$ZnCo_2O_4$/ZnO	5 A/g	304	5000	68.7	[42]
Peony-like $ZnCo_2O_4$	1 A/g	440	3000	67.7	[43]
$ZnCo_2O_4$ NAs/CC	2 A/g 3.6 mA/cm^2	1620	10,000	99.4	This work

(Fig. 9b) are shown in Fig. 9c. The results confirm that the $ZnCo_2O_4$ NAs/CC electrode has good mechanical stability.

In order to further explore the potential application of the as-prepared electrode, an asymmetric supercapacitor (ASC) device was assembled by CNTs/CC as the negative and $ZnCo_2O_4$ NAs/CC as the positive. Figure 10 shows the CV curves of the $ZnCo_2O_4$ NAs/CC electrode and CNTs/CC electrode performed in a three-electrode cell in 2 M KOH electrolyte at a scan rate of 15 mV/s. Figure 11 shows the charge and discharge curves of the CNTs. The charge

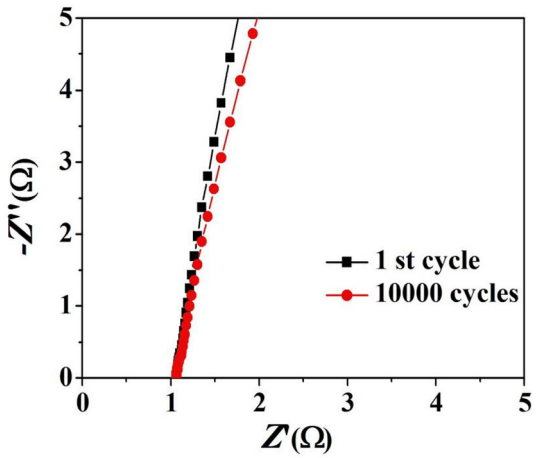

Fig. 7 The enlarged impedance image

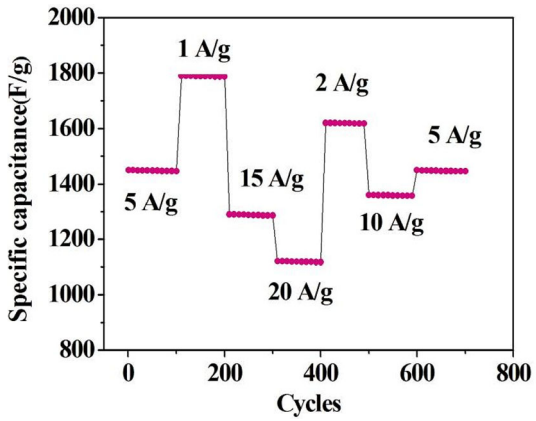

Fig. 8 Rate capability and cycle performance of the $ZnCo_2O_4$ NAs/CC electrode under different current densities

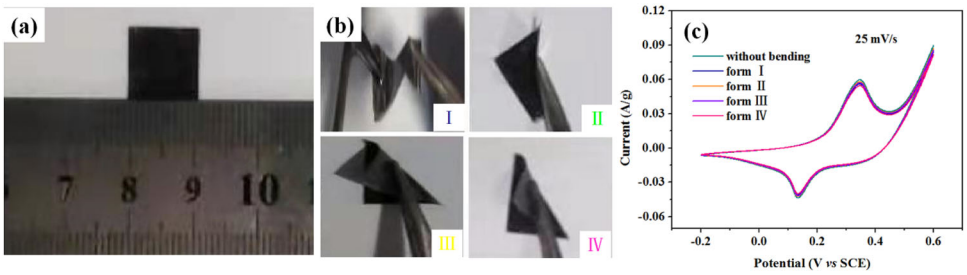

Fig. 9 **a** The digital picture of the $ZnCo_2O_4$ NSs/CC electrode. **b** $ZnCo_2O_4$ NSs/CC electrode undergoes four forms by bending and twisting. **c** CV curves of $ZnCo_2O_4$ NSs/CC electrode collected at 25 mV/s under different bending conditions

and the mass ratio between the negative and the positive are calculated according to the specific capacitance and potential windows range. Figure 12a exhibits the illustration of the ACS device. Figure 12b shows the CV curves of the $ZnCo_2O_4$ NAs/CC//CNTs/CC device at different potential windows. The ASC device can make the potential range for 1.8 V. But the CV curve at 0–1.8 V was unstable due to the hydrogen evolution. The results indicate that the stable potential window range is 0–1.6 V. Figure 12c shows the CV curves of the ASC device at different scan rates. The CV curves remain the same shape during the scan rate increase, indicating a good stability and fast transportation property of ions and electrons. Charge–discharge tests of the ACS device were explored at different current densities of 1, 2, 5, 8, 10, and 15 A/g as illustrated in Fig. 12d. The charge–discharge curves were nearly symmetrical, suggesting good electrochemical stability and capability. The specific capacitance of the device was calculated from the discharge curves and the results are shown in Fig. 12e. The specific capacitances of the

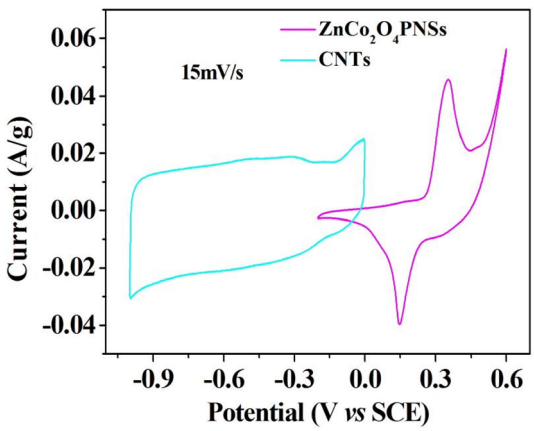

Fig. 10 CV curves of the $ZnCo_2O_4$ NAs/CC electrode and CNTs/CC electrode in a three-electrode cell at a scan rate of 15 mV/s

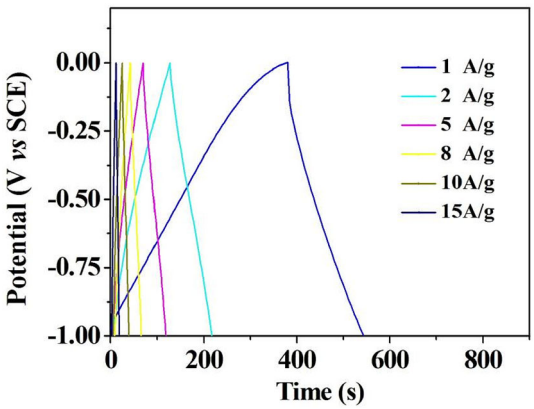

Fig. 11 Charge and discharge curves of CNTs at different densities

device are 131, 106, 94, 85, 75, and 70 F/g at the current density of 1, 2, 5, 8, 10, and 15 A/g, respectively. The Ragone plots of the ACS device are recorded in Fig. 12f. The device with high energy density and power density is calculated according to Eqs. 2 and 3, respectively. The maximum energy density of 47.1 Wh/kg is obtained at a current density of 1 A/g and the corresponding power density is 800 W/kg under the operating voltage of 1.6 V. This device possesses a maximum power density of 12,000 W/kg at the current density of 15 A/g and the energy density is 28.3 Wh/kg with the same potential window of 1.6 V. Finally, we compared this work with the reported work as shown in Fig. 11f [43–48].

4 Conclusion

In summary, the porous $ZnCo_2O_4$ NAs were successfully prepared by one-step hydrothermal method and succedent thermal treatment. The porous $ZnCo_2O_4$ NAs/CC electrode shows a high specific capacitance of 1790 F/g at the current density of 1

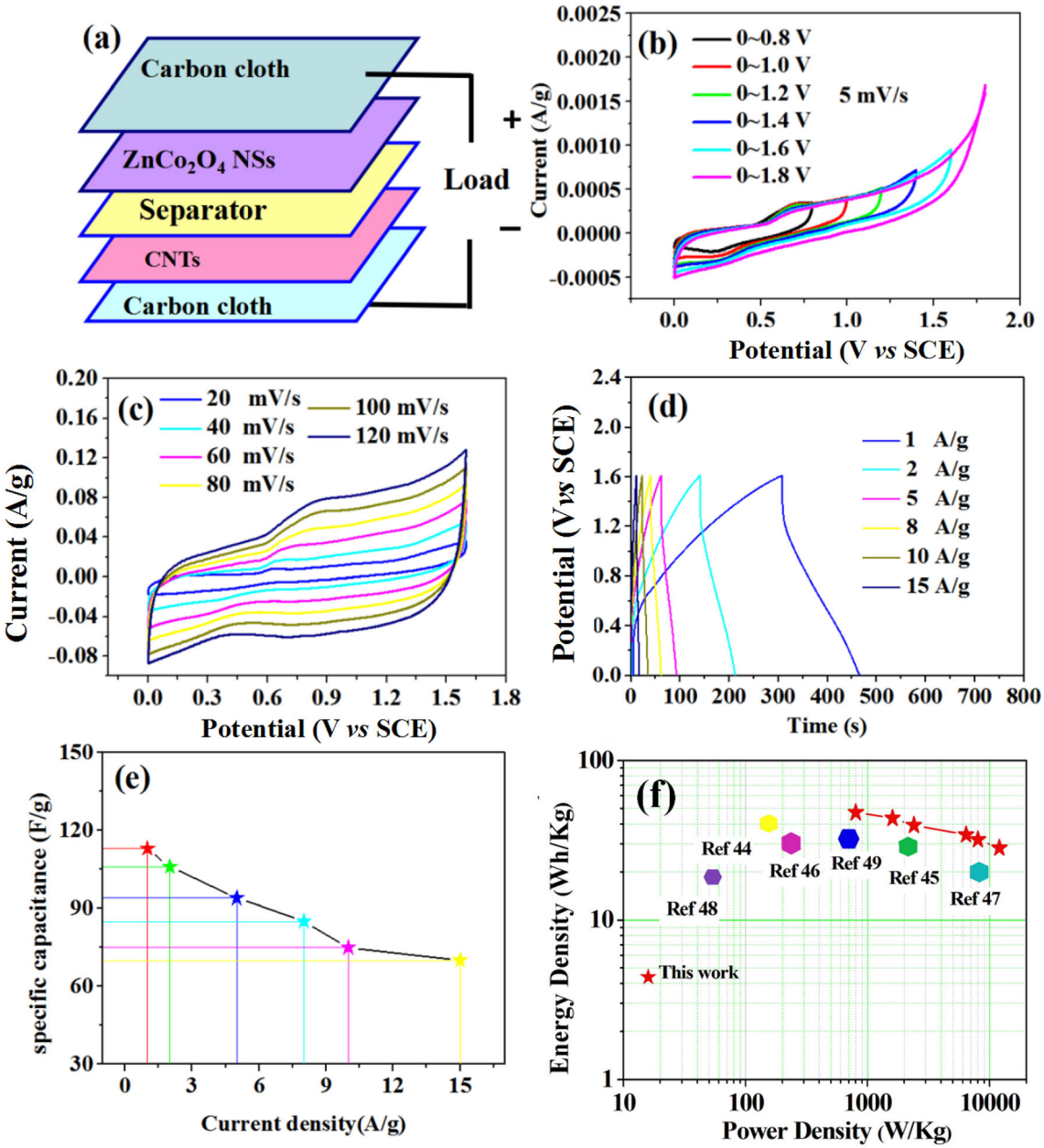

Fig. 12 **a** Schematic illustration for the $ZnCo_2O_4$ NSs/CC//CNTs/CC ACS device; **b** CV curves of the ACS device at different potential windows; **c** CV curves of the ACS device at different scan rate with potential window 0–1.6 V; **d** charge–discharge curves of the ACS device at different current densities; **e** specific capacitance of the ACS device at varied current densities; **and f** Ragone plots of the ACS device and other works

A/g and good cycle performance of 94% capacitance retention at the current density of 2 A/g after 10,000 cycles. The $ZnCo_2O_4$ NAs/CC//CNTs/CC ASC device demonstrates high energy density of 47.1 Wh/kg (at the power density of 800 W/kg) and power density of 12,000 W/kg (at the energy density of 28.3 Wh/kg). These results confirm that the as-prepared electrode and device will be promising energy storage devices in the future.

Acknowledgements

This research work was supported by the National Natural Science Foundation of China (No.52002099),

young scientists foundation from Harbin University of Commerce, China (2019CX28), and the Young scientific research item of Harbin University of Commerce, Heilongjiang province, China (No.2019DS084).

Author contributions

JW designed this experiment, carried out the electrochemical experiments, wrote the manuscript, and other analysis. CW and SW carried out the characterization tests, analyzed, wrote the results, and revised the manuscript. JC and XJ analyzed the characterization tests, wrote, and revised the manuscript. CW and JC analyzed and discussed the results.

Declarations

Conflict of interest The authors declare that they have no known competing financial interests or personal relationships that could have appeared to influence the work reported in this paper.

References

1. B. Dunn, H. Kamath, J.M. Tarascon, Science **334**, 928–935 (2011)
2. Q. Liu, X. Hong, X. Zhang, W. Wang, W. Guo, X. Liu, M. Ye, Chem. Eng. J. **356**, 985–993 (2019)
3. L.R. Hou, Y.Y. Shi, C. Wu, Y.R. Zhang, Y.Z. Ma, X. Sun, J.F. Sun, X.G. Zhang, C.Z. Yuan, Adv. Funct. Mater. **28**, 1705921 (2018)
4. A.M. Zardkhoshoui, S.S.H. Davarani, Dalton Trans. **49**, 10028–10041 (2020)
5. H. Liang, C. Xia, A.H. Emwas, D.H. Anjum, X. Miao, H.N. Alshareef, Nano Energy **49**, 155–162 (2018)
6. T. Xiong, T.L. Tan, L. Lu, W.S.V. Lee, J. Xue, Adv. Electron. Mater. **8**, 1702630 (2018)
7. Y. Zhu, Q. Zong, Q. Zhang, H. Yang, Q. Wang, H. Wang, Electrochim. Acta **299**, 441–450 (2019)
8. T. Chen, S. Li, P. Gui, J. Wen, X. Fu, G. Fang, Nanotechnology **29**, 205401 (2018)
9. R. Arian, A.M. Zardkhoshoui, S.S.H. Davarani, ChemElectroChem **7**, 2816–2825 (2020)
10. Y.Y. Chen, Y. Zhang, X. Zhang, T. Tang, H. Luo, S. Niu, Z.H. Dai, L.J. Wan, J.S. Hu, Adv. Mater. **29**, 1703311 (2017)
11. M. Li, J.S. Meng, Q. Li, M. Huang, X. Liu, K.A. Owusu, Z. Liu, L.Q. Mai, Adv. Funct. Mater. **8**, 1802016 (2018)
12. S.Y. Zhou, S. Wang, S.J. Zhou, H.B. Xu, J.P. Zhao, J. Wang, Y. Li, Nanoscale **12**, 8934–8941 (2020)
13. H.B. Xu, L.T. Gong, S.Y. Zhou, New J. Chem. **44**, 2236–2240 (2020)
14. A.M. Zardkhoshoui, S. Saeed, H. Davarani, Nanoscale **12**, 1643–1656 (2020)
15. B. Ameri, A.M. Zardkhoshoui, S. Saeed, H. Davarani, Sustain. Energy Fuels **4**, 5144–5155 (2020)
16. Z.G. Zhang, X. Huang, H.X. Wang, S.H. Teo, T.L. Ma, J. Alloys Compd. **771**, 274–280 (2019)
17. J.S. Lin, L. Yao, Z.L. Li, P.X. Zhang, W.H. Zhong, Q.H. Yuan, L.B. Deng, Nanoscale **11**, 3281–3291 (2019)
18. W.D. He, Z.F. Liang, K.Y. Ji, Q.F. Sun, T.Y. Zhai, X.J. Xu, Nano Res. **11**, 1415–1425 (2018)
19. A.M. Zardkhoshoui, S. Saeed, H. Davarani, Chem. Eng. J. **402**, 126–241 (2020)
20. A.M. Zardkhoshoui, S. Saeed, H. Davarani, Nanoscale **5**, 1–36 (2020)
21. A.M. Zardkhoshoui et al., J. Power Sources **450**, 227–691 (2020)
22. S.S. Karade, S. Lalwani, J.H. Eum, H. Kim, Sustain. Energy Fuels **4**, 1–32 (2020)
23. S. Raj, S.K. Srivastava, P. Kar, P. Roy, Electrochim. Acta **302**, 1–33 (2019)
24. P.A. Shinde, N.R. Chodankar, S. Lee, E. Jung, S. Aftab, Y.K. Han, S. Jun, Chem. Eng. J. **405**, 1–13 (2021)
25. H. Chen, G.H. Jiang, W.J. Yu, D.P. Liu, Y.K. Liu, A.L. Li, Q. Huang, Z.Z. Tong, J. Mater. Chem. A **4**, 5958–5965 (2016)
26. V. Venkatachalam, A. Alsalme, A. Alswieleh, R. Jayavel, Chem. Eng. J. **321**, 474–483 (2017)
27. S.J. Patil, J. Park, D.W. Lee, IOP Conf. Ser.: Mater. Sci. Eng. **282**, 1–6 (2017)
28. B. Liu, J. Zhang, X.F. Wang, G. Chen, D. Chen, C.W. Zhou, G.Z. Shen, Nano Lett. **12**, 3005–3011 (2012)
29. X.M. Wu, L. Meng, Q.G. Wang, W.Z. Zhang, Y. Wang, Mater. Lett. **234**, 1–4 (2019)
30. Y.P. Huang, Y.E. Miao, H.Y. Lu, T.X. Liu, Chem. Eur. J. **21**, 10100–10108 (2015)
31. Q.H. Wang, Y.X. Zhu, J. Xue, X.S. Zhao, Z.P. Guo, C. Wang, ACS Appl. Mater. Interfaces **8**, 17226–17232 (2016)
32. Q.H. Wang, J.L. Du, Y.X. Zhu, J.Q. Yang, J. Chen, C. Wang, L. Li, L.F. Jiao, J. Power Sources **284**, 138 (2015)
33. H. Niu, X. Yang, H. Jiang, D. Zhou, X. Li, T. Zhang, J.Y. Liu, Q. Wang, F.Y. Qu, J. Mater. Chem. A **3**, 24082 (2015)
34. J.K. Sun, P. Zan, L. Ye, X.J. Yang, L.J. Zhao, J. Mater. Chem. A **5**, 9815 (2017)
35. H. Wu, Z. Lou, H. Yanga, G.Z. Shen, Nanoscale **7**, 1921–1926 (2015)
36. S.J. Peng, L.L. Li, H.B. Wu, S. Madhavi, X.W. Lou, Adv. Energy Mater. **5**, 1401172 (2015)

37. M.C. Liu, L.B. Kong, C. Lu, X.J. Ma, X.M. Li, Y.C. Luo, L. Kang, J. Mater. Chem. A **1**, 1380–1387 (2013)
38. C. Qing, C.X. Yang, M.Y. Chen, W.H. Li, S.Y. Wang, Y.W. Tang, Chem. Eng. J. **354**, 182–190 (2018)
39. Q.H. Wang, L.X. Zhu, L.Q. Sun, Y.C. Liu, L.F. Jiao, J. Mater. Chem. A **3**, 982–985 (2015)
40. F. Nti, D.A. Anang, J.I. Han, J. Alloys Compd. **742**, 342–350 (2018)
41. L. Huang, W. Zhang, J.W. Xiang, H.H. Xu, G.L. Li, Y.H. Huang, Sci. Rep. **6**, 31465 (2016)
42. J.L. Sun, S.S. Li, X.R. Han, F. Liao, Y.F. Zhang, L. Gao, H.Y. Chen, C.J. Xu, Ceram. Int. **45**, 12243–12250 (2019)
43. Y.Y. Shang, T. Xie, Y.S. Gai, L.H. Su, L.Y. Gong, H.J. Lv, F.Y. Dong, Electrochim. Acta **253**, 281–290 (2017)
44. X.Z. Li, M.Y. Zhang, L.L. Wu, Q.S. Fu, H. Gao, J. Alloys Compd. **773**, 367–375 (2019)
45. P. Zhang, J.Y. Zhou, W.J. Chen, Y.Y. Zhao, X.M. Mu, Z.X. Zhang, X.J. Pan, E.Q. Xie, Chem. Eng. J. **307**, 687–695 (2017)
46. P.J. Wang, H.R. Cai, X.L. Li, Y.F. Yang, G. Li, J.L. Xie, H.C. Xia, P.H. Sun, D.S. Zhang, J. Xiong, New J. Chem. **43**, 7065–7073 (2019)
47. W. Qin, J.L. Li, X.Y. Liu, N.F. Zhou, C. Wu, M. Ding, C.K. Jia, J. Colloid Interface Sci. **554**, 125–132 (2019)
48. D. Cheng, Y.F. Yang, J.L. Xie, C.J. Fang, G.Q. Zhang, J. Xiong, J. Mater. Chem. A **3**, 14348–14357 (2015)